Journal of Materials Chemistry A

ROYAL SOCIETY OF CHEMISTRY

PAPER

View Article Online
View Journal | View Issue

Cite this: J. Mater. Chem. A, 2020, 8, 13630

Frequency switchable correlated transports in perovskite rare-earth nickelates†

Jikun Chen, *[a] Haifan Li,[a] Jiaou Wang,[b] Xinyou Ke,[c] Binghui Ge, [d] Jinhao Chen,[a] Hongliang Dong,[e] Yong Jiang*[a] and Nuofu Chen*[f]

While electron correlations were previously recognized to result in direct current (DC) transportation properties beyond-conventional (*e.g.*, metal-to-insulator transitions, bad metal, thermistors), their respective influences on the alternating current (AC) transport are largely overlooked. Herein, active regulation of the electronic functionalities of d-band correlated rare-earth nickelate ($ReNiO_3$) thin films, by simply utilizing their electronic responses to AC-frequencies (f_{AC}) is demonstrated. Assisted by temperature dependent near edge X-ray absorption fine structure analysis, positive temperature dependences in the Coulomb viscosity of $ReNiO_3$ were discovered, which moderate their AC impedance ($R' + iR''$). Distinguished crosslinking among R'–f_{AC} measured in nearby temperatures is observed that differs to conventional oxides. This enables active adjustability in correlated transports of $ReNiO_3$, among NTCR-, T_{Delta}- and PTCR-thermistors, *via* f_{AC} from the electronic perspective without varying materials or device structures. Furthermore the T_{Delta}–f_{AC} relationship can be widely adjusted *via* the *Re* composition and interfacial strains. The AC-frequency sensitivity discovered in $ReNiO_3$ leads the way to a new freedom in regulating and switching the device working states beyond the present semiconductor technologies. It opens up a new model for enriching novel electronic applications in automatic transmission, artificial intelligence in sensing temperatures or thermal perturbations.

Received 5th May 2020
Accepted 16th June 2020

DOI: 10.1039/d0ta04663a

rsc.li/materials-a

1. Introduction

The d-band electron correlation within transitional oxides and their respective applications in electronic devices beyond semiconductors is a central idea in modern condensed matter physics. The Coulomb energy domination in electronic orbital configurations and transitions enriches distinguished electronic functionalities, *e.g.*, hydrogenation-induced quantum phase transitions,[1–5] metal to insulator transitions (MIT),[6–12] broad temperature range thermistors,[13,14] and bad metal transport.[15] The rare-earth nickelates ($ReNiO_3$) is one representative of the d-band correlated perovskites that exhibit exceptionally sensitive electronic structures to external stimulus, such as temperature,[6,9] lattice distortion,[6,8] charge polarization,[7] and chemical atmosphere.[1–5] In particular, the recent discoveries of the hydrogen induced electron localization within $ReNiO_3$ enables new electronic and Mottronic applications in ocean current sensing,[1] synaptic plasticity,[5] logic/memory devices,[4] bio-sensing,[2] and energy conversions.[3]

Nevertheless, the previously achieved electronic and Mottronic functionalities within d-band correlated semiconductors (*e.g.*, $ReNiO_3$) mainly rely on electronic responses to direct current (DC) signals,[1–15] and in this situation, the as-achieved functionalities are passively determined by the material's properties. In contrast, the utilization of the alternating current (AC) electronic transportations in correlated electronic devices remains yet to be explored. For example, the insulating orbital configuration for $ReNiO_3$ ($Ni^{3+}t_{2g}^6e_g^{1+\Delta}$ + $Ni^{3+}t_{2g}^6e_g^{1-\Delta}$) was recognized to gradually transit with temperature,[6,13] whereas more abrupt orbital transitions towards the metallic phase ($Ni^{3+}t_{2g}^6e_g^1$) are triggered by elevating the temperature (T) across a critical point (T_{MIT}).[6] Whilst these orbital transitions beyond conventional semiconductors were previously recognized to enable DC-electronic properties such as thermistor behavior and MIT,[6,13] their respective regulations of the AC-electronic functionalities remain unknown. It is worth noting that their Coulomb energy dominated orbital configuration will result in synergistic variations in their impedance ($R' + iR''$), as related to not only temperatures but also frequencies (f_{AC}). From

[a]Beijing Advanced Innovation Center for Materials Genome Engineering, School of Materials Science and Engineering, University of Science and Technology Beijing, Beijing 100083, China. E-mail: jikunchen@ustb.edu.cn; yjiang@ustb.edu.cn

[b]Beijing Synchrotron Radiation Facility, Institute of High Energy Physics, Chinese Academy of Sciences, Beijing 100049, China

[c]Department of Mechanical and Aerospace Engineering, Case Western Reserve University, Cleveland, OH 44106, USA

[d]Institute of Physical Science and Information Technology, Anhui University, 230601, Heifei, Anhui, China

[e]Center for High Pressure Science and Technology Advanced Research, Shanghai 201203, China

[f]School of Renewable Energy, North China Electric Power University, Beijing 102206, China. E-mail: nfchen@ncepu.edu.cn

† Electronic supplementary information (ESI) available. See DOI: 10.1039/d0ta04663a

this perspective, the previously demonstrated MIT and thermistor behaviors are barely the tip of the iceberg of the electronic functionalities within ReNiO$_3$, when their impedances are overwhelmed by DC-conduction (also the case for using low f_{AC}). There is no doubt, that exploring the beyond conventional AC-transports at a higher f_{AC} for correlated ReNiO$_3$ will open new fields for the discovery of new electronic functionalities beyond the present knowledge. More importantly, it will also clarify the utilization of f_{AC} as an additional way to achieve active regulation of the working states of electronic devices from the electronic perspective without changing the material constitutions or the device structures.

Herein, the distinguished T and f_{AC} dependence in the AC transport for the correlated ReNiO$_3$ thin films is demonstrated, and this enables actively switchable electronic functionalities as controlled by f_{AC} without varying the materials' and device structures. By simply increasing the input f_{AC} of the detection AC signal, the electronic transportation behavior of ReNiO$_3$ transformed from a negative temperature coefficient of resistance (NTCR) thermistor at low f_{AC}, to a delta-temperature (T_{Delta}) thermistor at a middle-range f_{AC}, and further towards a positive temperature coefficient of resistance (PTCR) thermistor at high f_{AC}. Assisted by temperature dependent near edge X-ray absorption fine structure (NEXAFS) analysis, it was demonstrate experimentally that the temperature induced gradual orbital transitions within the insulating phase of ReNiO$_3$. From the perspective of materials' design, it was further shown that the critical transition frequencies ($f_{NTCR-Delta}$ and $f_{Delta-PTCR}$) within a given range of temperature can be widely adjustable *via* the rare-earth composition (*Re*) or by imparting interfacial strains.

2. Materials and methods

The thin films including SmNiO$_3$, EuNiO$_3$, HoNiO$_3$ and Sm$_{0.75}$Nd$_{0.25}$NiO$_3$ were grown on LaAlO$_3$ (001) substrate using a chemical spin coating procedure followed by annealing under high oxygen pressure according to methods in previous reports.[13,14] In brief, the chemical precursors of $Re(NO_3)_3$ and $Ni(CH_3COO)_2$ were mixed together at a nominal stoichiometry and the resulting solution, was then spin coated onto LaAlO$_3$ (001) single crystal substrates. Next, the spin coated ReNiO$_3$/LaAlO$_3$ were annealed at 800 °C under a high pressure oxygen atmosphere (from 8 MPa to 15 MPa). In addition, pulsed laser deposition (PLD) was also used to grow a coherent SmNiO$_3$ on SrTiO$_3$ (001) substrate. In brief, a ceramic target was ablated by a 248 nm laser beam at 20 Pa O_2 inside a vacuum chamber, and the substrate was heated up to 700 °C during the film deposition.

The interfacial morphology of the as-grown thin films was observed by high-angle annular dark-field (HAADF) and annular bright-field (ABF) scanning transmission electron microscopy (STEM) performed on a Jeol JEM-ARM200F TEM operated at 200 kV with a cold field emission gun and aberration correctors for both probe-forming and imaging lenses. The in-plane lattice relationship between the film and substrate was further characterized by performing reciprocal space mapping (RSM) by tracing the [114] reciprocal space vectors of the substrate. The temperature dependent near edge X-ray absorption fine structure (TDNEXAFS) was performed at the Beijing Synchrotron Radiation Facility (Institute of High Energy Physics, Chinese Academy of Sciences, Beijing 100049, China). The temperature dependent direct current resistance above room temperature was characterized by using a commercialized CTA-system. The frequency dependent impedance measurements of the as-grown thin films were performed using a Keithley 4200 semiconductor characterization system, where the temperature was controlled by a liquid nitrogen cooling system. The magnitude of the impedances (R' and R'') and the imparted AC-frequency were both within the normal characterization range of the Keithley 4200. At a low AC-frequency (100 Hz), the R'–T tendency was similar to the respective measurement using DC sources. Fig. S1 (ESI†) shows the schematic illustration for characterizing the AC-impedance. A two point contact was used for the characterization, which is how it will be used as a thermistor.

3. Results and discussions

General concept

The DC electronic conductivity (σ_{DC}) of ReNiO$_3$ as previously described by the Drude model is written as: $\sigma_{DC} = \frac{nq^2\tau}{m^*}$, where n, q, m^* represent the concentration, charge and effective mass of the carrier, respectively, and τ is the life time between the carrier scatterings. Whilst ReNiO$_3$ was previously demonstrated to be a bad metal with a saturating τ–T tendency,[15] the temperature dependence in σ_{DC} originated from the n–T and m^*–T tendencies. Thermal activation of the carriers is well recognized, as the concentration of the semiconductors follows: $n_{(T)} = \frac{n_0\ \exp(-E_g)}{k_B T}$, where k_B is the Boltzmann constant, E_g is the energy band gap and n_0 is a constant initial carrier concentration. Nevertheless, the potential temperature dependency in m^* had previously been overlooked.

In contrast to conventional semiconductors, the carrier conduction within the insulating phase of ReNiO$_3$ was dominated by strong interactions with the lattice charge associated to the NiO$_6$ octahedron and followed a hopping mechanism.[16] As illustrated in Fig. 1a, the carrier hopping between the adjacent NiO$_6$ octahedrons was expected to result in instantaneous charge polarizations from the electrical field which drags the hopping carriers. This effect is analogous to increasing the viscosity of the carrier transport within semiconductors, *e.g.*, by prohibiting the acceleration of carriers under an externally imparted electrical field, and thereby enlarging m^*. Therefore, the potential m^*–T tendencies within ReNiO$_3$ can be understood to be a sign of temperature increased Coulomb viscosity (η) of the carrier transport, as defined here to be $m^*_{(T)} = \eta_{(T)} m^*_0$. Apart from moderating the temperature dependence of the DC-transportations, the $\eta_{(T)}$ was also expected to influence the frequency responses in the impedance of ReNiO$_3$. For example, enlarging η (or m*) reduced the phase difference between the hopping carriers and the lattice polarizations, which increased the relaxation frequency (f_0) from the perspective of the AC-transports.[17–24] Although the NTCR thermistor DC-transport is

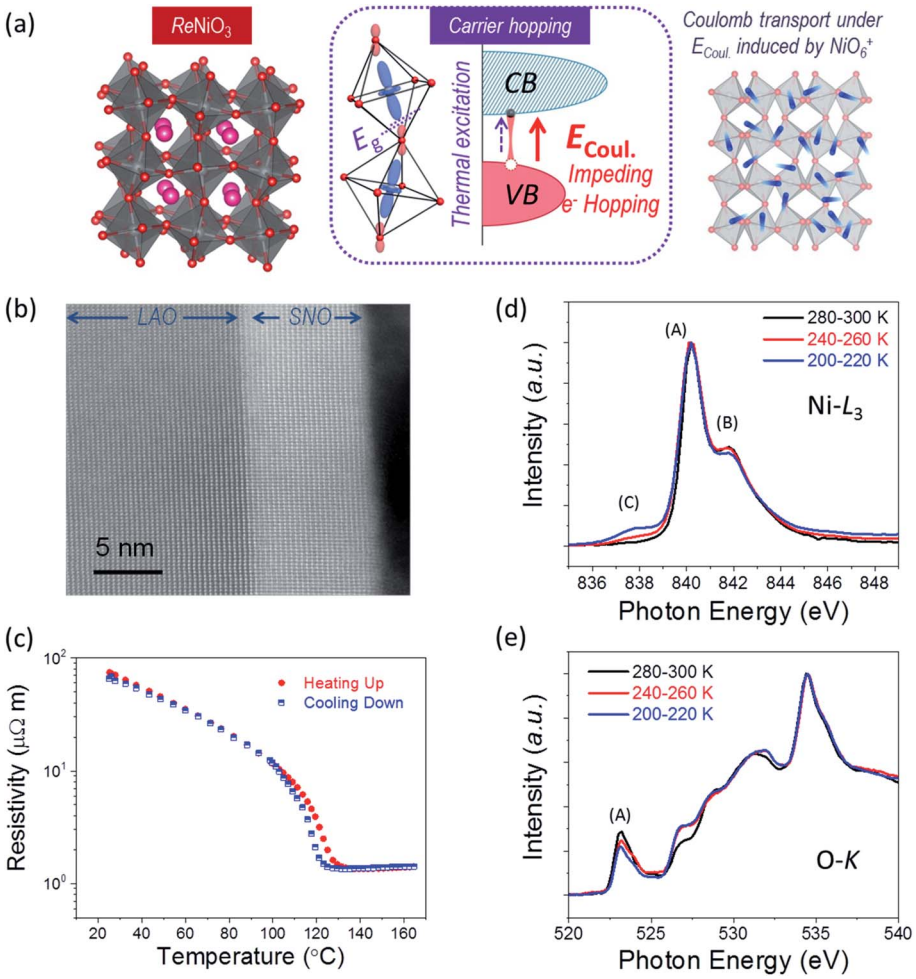

Fig. 1 (a) Schematic illustrations of the crystal structure and lattice Coulomb interaction regulated carrier hopping for *Re*NiO_3. (b) Interfacial cross-section morphology for the as-grown $SmNiO_3/LaAlO_3$. (c) Temperature dependence of $SmNiO_3/LaAlO_3$ measured *via* both heating up and cooling down processes that demonstrate that a sharp metal to insulator transition was achieved. (d and e) Temperature dependent near edge X-ray absorption fine structure analysis of (d) the Ni-L_3 edge and (e) the O-K edge of $SmNiO_3$ at various temperatures.

already known for the insulating phase of *Re*NiO_3, further explorations of their AC-impedance behaviors as related to both temperature and frequency are required.

Materials' growth and electronic structures

Following the previously discussed considerations, *Re*NiO_3 thin films were grown epitaxially, with compositions including $SmNiO_3$, $NdNiO_3$, $EuNiO_3$, $HoNiO_3$, and $Sm_{0.75}Nd_{0.25}NiO_3$ on single crystalline $LaAlO_3$ and $SrTiO_3$ substrates, using solution-based chemical spin coating followed by high oxygen pressure annealing according to methods in previous reports.[13,14] More experimental details are described in Section A for the ESI.† Fig. 1b demonstrates the cross section morphology of the as-grown $SmNiO_3/LaAlO_3$ (001), where a coherent interface between the film and substrate was observed. The $SmNiO_3/LaAlO_3$ sample exhibited sharp MIT behavior with a T_{MIT} of ~120 °C, as demonstrated in Fig. 1c. To characterize the temperature induced variations in the electronic structure of the as-grown $SmNiO_3/LaAlO_3$ (001), TDNEXAFS was performed to probe its Ni-L and O-K edges at various temperatures, and the results are shown in Fig. 1d and e, respectively. Reducing the temperature decreased the relative intensity in the proportion of sub-peaks (B) within the Ni-L_3 spectrum (see Fig. 1d), whereas the pre-peak (A) in the O-K edge (from the $d^8\underline{L}$ configuration) was also decreased (see Fig. 1d). These observations indicate the elevation in the insulating $t_{2g}^6e_g^2$ (Ni^{2+}) ground state orbital configuration compared to metallic $t_{2g}^6e_g^2$ (Ni^{2+}) $t_{2g}^6e_g^1$ (Ni^{3+})[25,26] with descending temperature. Similar observations in the NEXAFS spectrum were previously observed when the insulating phase of *Re*NiO_3 was strengthened by reducing the size of *Re*[13] or imparting tensile lattice distortions.[27] It is also interesting to note that an additional sub-peak (C) arose prior to the main peak (A) in the Ni-L_3 spectrum at low temperatures, indicating the partial dragging of empty orbitals towards a lower energy level. This observation was consistent with the situation when the conduction band edge caves in downwards that increases the band curvature and reduces the effective mass, resulting in a positive η–T tendency.

Delta-temperature thermistor behavior achieved in $SmNiO_3$

The impedances for $SmNiO_3/LaAlO_3$ (001) measured at various temperatures, are plotted as a function of the AC frequency in Fig. 2a and b for R' and R'', respectively, and their Nyquist plots, are shown in Fig. S2 (ESI†), exhibited only one circle, and this indicated that the impedance characterization is dominated by $ReNiO_3$ rather than by the interfaces or grain boundaries. At each temperature, R' and R'' follows the following equations:[17]

$$R' = \frac{\varepsilon_0\sigma_{DC}}{\sigma_{DC}{}^2C_0 + (2\pi f_{AC})^2\varepsilon_0{}^2\varepsilon'^2C_0} \quad (1)$$

$$R'' = \frac{\varepsilon'}{2\pi f_{AC}C_0\varepsilon'^2 + C_0\sigma_{DC}{}^2(2\pi f_{AC}\varepsilon_0{}^2)^{-1}} \quad (2)$$

where ε_0 and ε' represent the vacuum and relative permittivity, respectively, whereas C_0 is the geometric capacitance parameter at a constant value. At a low f_{AC}, the carrier transport was dominated by σ_{DC} similar to DC-transport, in which situation R' shows a plateau magnitude of $R_{DC} = \varepsilon_0(\sigma_{DC}C_0)^{-1}$ whereas R'' is small. Increasing the f_{AC} will weaken the carrier shielding of the lattice polarization and enlarge R'' until the maximum magnitude is reached at its relaxation frequency, f_0 $\left(e.g., f_0 = \frac{\sigma_{DC}}{2\pi\varepsilon_0\varepsilon'}\right)$, in which situation R'' reaches its maximum. Meanwhile, the term $(2\pi f_{AC})^2\varepsilon_0{}^2\varepsilon'^2C_0$ in the denominator of R' starts to dominate its magnitude for $f_{AC} > f_0$. As a result, the R'–f_{AC} tendency deviates from the previous plateau at a low frequency and shows a tendency to reduce as it gradually reaches a $f_{AC}{}^{-2}$ tendency. Plotting R'' as a function of R' at various f_{AC}, a semi-circle known as the core–core plot is obtained. By further comparing the above understanding with the results shown in Fig. 2a, b and S2 (ESI†), it can be seen that the impedance properties for the insulating phase of $SmNiO_3$ are similar to those of conventional dialectic materials with a high DC-current leakage, and this is consistent with their theoretical expressions as demonstrated by eqn (1) and (2).

Nevertheless, it is interesting to note the reverse tendencies in the temperature dependences of R' and f_0. For example, by

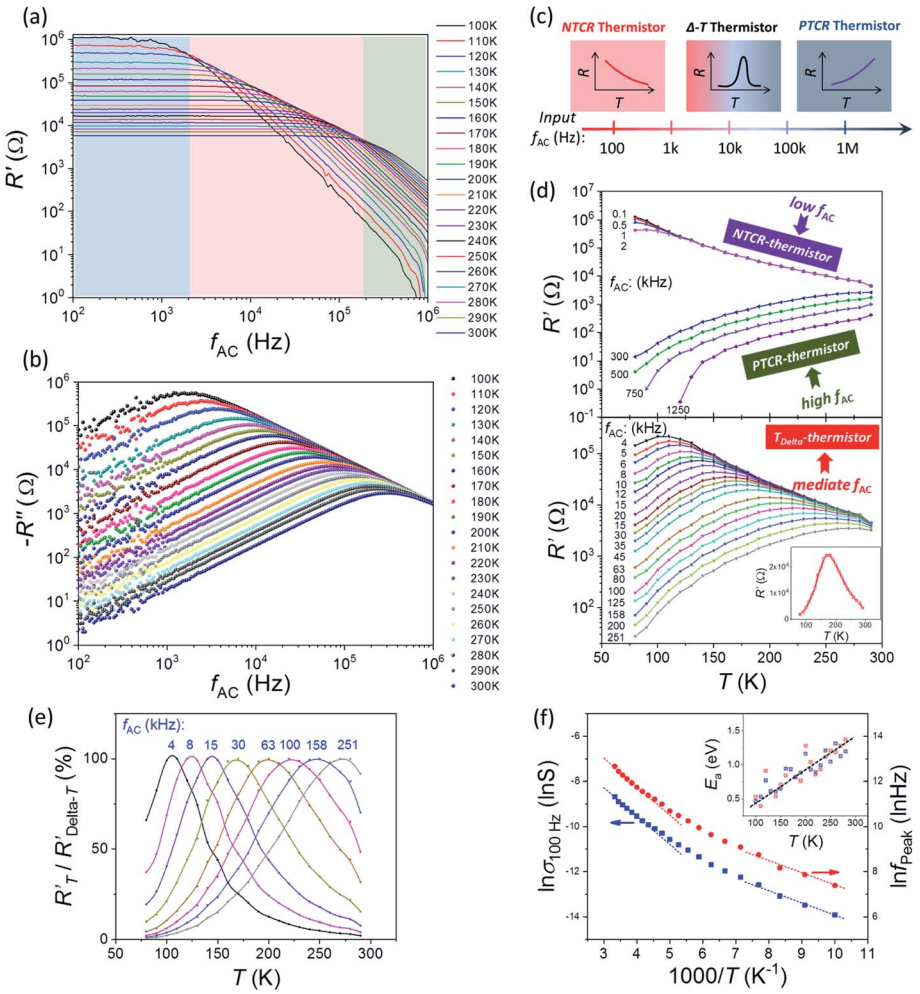

Fig. 2 (a and b) The (a) real and (b) imaginary part of the impedance measured for $SmNiO_3/LaAlO_3$ as a function of frequency of the input detection AC-signal at various temperatures. (c) Illustration of the AC-frequency determination and switchability among NTCR, T_{Delta}- and PTCR thermistor functionalities. (d) Temperature dependence in resistance (R'–T) measured at various AC-frequencies. (e) Relative resistance compared to the maximum magnitudes at T_{Delta} at various AC-frequencies. (f) The $\ln(\sigma_{100\ Hz})$–$1000/T$ and $\ln(f_0)$–$1000/T$ tendencies that are used to calculate the temperature dependence in the activation energy (E_a) from the perspective of both the DC and AC transportations.

further varying the temperature, a negative R'–T tendency was observed at low f_{AC}, whereas the respective f_0–T tendency was positive. Thus, the R'–f_{AC} curves measured at adjacently measured temperatures were indeed crosslinked, as shown by the region marked in pink in Fig. 2a. Such pronounced crosslinking in R'–f_{AC} measured at nearby temperatures had not been observed previously in other functional oxides, such as spinal type ferrites (*e.g.*, $NiFe_2O_4$),[18] hexaferrite (*e.g.*, $Sr_3Co_2Fe_{24}O_{41}$),[19] titanate perovskite (*e.g.*, W-doped $CaBi_4Ti_4O_{15}$),[20] lead zirconate titanate,[21] manganese perovskite (*e.g.*, $La_{0.7}Sr_{0.3}MnO_3$ and $La_{0.5}Ca_{0.5-x}Ag_xMnO_3$),[22,23] and $BiFeO_3$.[24]

Accordingly, detection of R'–T utilizing a specific f_{AC} within the crosslinking region achieved the as-proposed T_{Delta}-thermistor transport, whereas reducing or elevating f_{AC} achieves the NTCR and PTCR thermistor functionalities,[28,29] respectively, as illustrated in Fig. 2c. Fig. 2d demonstrates the representative R'–T tendencies for $SmNiO_3/LaAlO_3$ at various values of f_{AC}. For applying low f_{AC} below kHz, a negative R'–T tendency, behaving as an NTCR thermistor, with a NTCR above 2% K^{-1} was observed across the entire target temperature range from 80 K to 300 K. In contrast, applying high f_{AC} exceeding 300 kHz enabled the PTCR thermistor functionality, as a positive R'–T tendency was observed within the same target temperature range. By imparting an intermediate f_{AC} in between, a delta-like R'–T tendency behaving as a T_{Delta}-thermistor was obtained, in which case R' firstly increased with T until reaching the maximum at T_{Delta} and afterwards reduced rapidly. The maximum point in the R' tendency could be used to lock in the temperature range near T_{Delta}, and this was also actively adjustable within the entire temperature range *via* f_{AC}, *e.g.*, increasing f elevated T_{Delta} which is more clearly demonstrated in Fig. 2e. The previous observations are confirmed to be associated to the $SmNiO_3$ film material, rather than the external circuit or the substrate (see confirmation experiments demonstrated in Fig. S3 and S4, ESI†).

Temperature dependence in Coulomb viscosity

It is worth noting that the carrier transportation associated with the insulating phase was found to be complicated. For example, temperature may trigger the variations in carrier type and concentration as reported for the insulating phase of $SmNiO_3$,[32] whereas a gradual transition in their band gap was also expected.[14] Herein, the carrier activation energy (E_a) was further estimated from the temperature dependence of the plateau resistance at low f_{AC} (similar to DC resistance) and also the relaxation frequency in R'', as shown in Fig. 2f. For both situations, E_a was temperature dependent, and roughly followed a linear relationship as shown in the inset of Fig. 2f. The E_a–T dependence as observed in $ReNiO_3$ was in contrast to the ones previously observed for other functional oxides, *e.g.*, doped ZnO,[17] $Sr_3Co_2Fe_{24}O_{41}$ (ref. 19) $CaBi_4Ti_4O_{15}$,[20] $La_{0.7}Sr_{0.3}MnO_3$

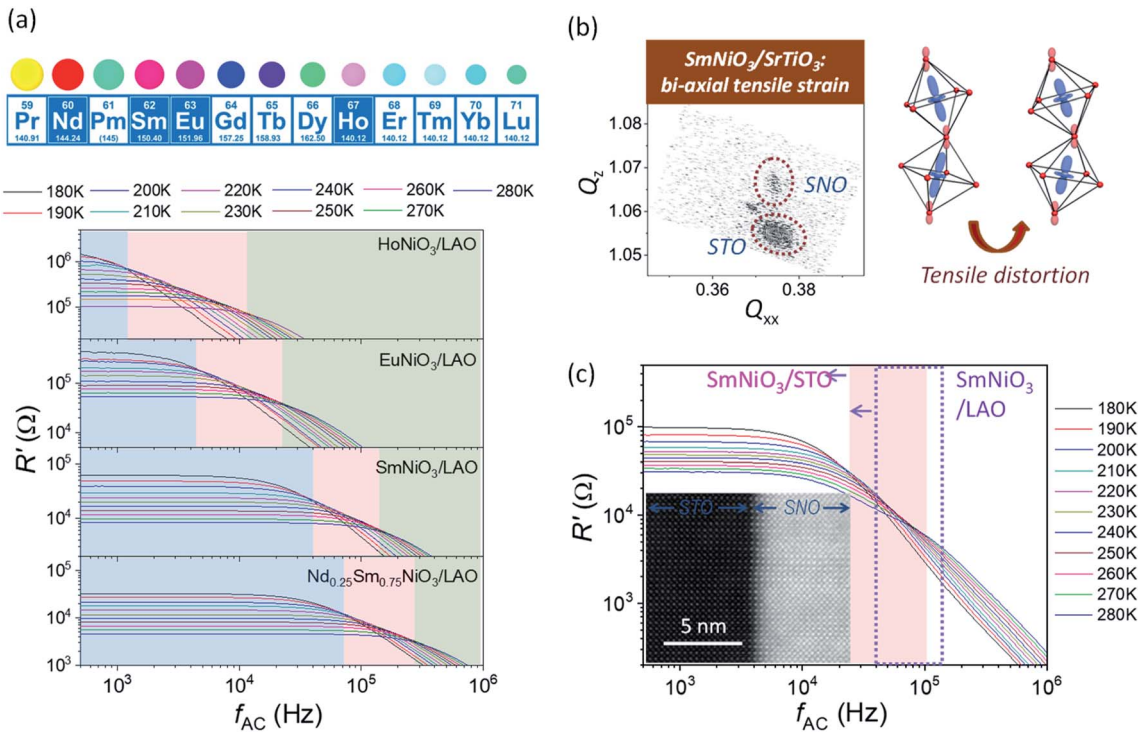

Fig. 3 (a) Comparing the resistance to AC frequency (R'–f_{AC}) tendency measured at various temperatures for $ReNiO_3/LaAlO_3$ with various rare-earth compositions including $Nd_{1/4}Sm_{1/3}$, Sm, Eu, Ho. (b) Reciprocal space mapping (RSM) for the coherent pulsed laser deposition $SmNiO_3$ on $SrTiO_3$ (001) substrate, in which biaxial tensile distortion is imparted to the as-grown thin film. (c) Comparing the resistance to AC frequency (R'–f_{AC}) tendency measured at various temperatures for the biaxial tensile strained $SmNiO_3/SrTiO_3$ to the one for $SmNiO_3/LaAlO_3$ at a slightly biaxial compressive distortion. The inset in (c) demonstrates that a coherent interface is achieved for $SmNiO_3/SrTiO_3$ that further confirms the preservation of the tensile interfacial strain.

(ref. 22) and $BiFeO_3$.[24] Furthermore from the quasi-linear E_a–T tendency, differential equation groups were established to calculate the expressions of Coulomb viscosity for $SmNiO_3$/$LaAlO_3$, and more details demonstrated this are given in Section C of the ESI.† A temperature dependence of $\eta_{(T)} \propto T^{\beta}$ ($\beta = 4$) was obtained that indicated an enlarged carrier viscosity within $SmNiO_3$ with the elevated temperature. This was expected to result from the enhanced Coulomb interactions among the carrier transports during the temperature induced gradual orbital transportations within the insulating phase as indicated by the NEXAFS results shown in Fig. 1d and e.

Because the energy band gap of $ReNiO_3$ was unlikely to be widened by elevating the temperature, it was expected that the role of the positive temperature dependence in η (or m^*) could not be neglected in the regulation of the carrier transport. For example, elevating the temperature was expected to significantly excite the carrier hopping together with the instantaneous polarized NiO_6, resulting in the higher viscosity of the carrier transport. This increased the critical relaxation frequency in the impedance, and caused right-shifting of the R'–f_{AC} curve with the elevation in temperature. In the meantime, the magnitude in plateau R' at low frequency (equal to the DC resistance) would be reduced, resulting in crosslinking between the R'–f curves measured at nearby ranges of temperatures.

Extending the investigations to other $ReNiO_3$

The investigations were further extended to the insulating phases of other $ReNiO_3$ (*e.g.*, $EuNiO_3$, $Sm_{3/4}Nd_{1/4}NiO_3$ and $HoNiO_3$) and achieved similar functionalities, as their temperature dependent R'–f_{AC} and R''–f_{AC} curves demonstrated in Fig. 3a and S5 (ESI†), respectively. It is worth noting that reducing the size of the rare-earth elements shifted the crosslinking R'–f_{AC} region towards a lower frequency, and this was expected to be caused by the strengthening of the insulating phase to reduce both the carrier density and viscosity. In addition, a similar effect was achieved when imparting biaxial tensile interfacial strain upon the co-lattice grown $SmNiO_3$ on $SrTiO_3$, in which case the insulating phase of $ReNiO_3$ could also be strengthened.[27,30,31] For example, the $SmNiO_3$/$SrTiO_3$ sample grown by pulsed laser deposition exhibited the same in-plane lattice constants between the film and substrate, as demonstrated by its RSM as shown in Fig. 3b and the interfacial morphology shown in the inset of Fig. 3c. Such tensile strained $SmNiO_3$/$SrTiO_3$ exhibited a crosslinked region in R'–f_{AC} at a lower frequency range, compared to $SmNiO_3$/$LaAlO_3$, as shown in Fig. 3c (see respective R''–f_{AC} in Fig. S6, ESI†). It is worth noting that by either reducing the size of *Re* or imparting tensile strains, the insulating phase of $ReNiO_3$ will be strengthened. As a result, it was easier for the phase difference between the carrier and lattice charge to occur *via* lower frequencies.

From the previously described demonstrations, it can be seen that the frequency switchable thermistor functionalities can be generally achieved in the insulating phase of $ReNiO_3$ with various rare-earth compositions, lattice distortions, and grown using different deposition approaches (*e.g.*, both PLD and spin coating). In contrast, similar effects were not observed for the metallic phase of $ReNiO_3$, as can be seen for the R'–f_{AC} tendency which is shown in Fig. S7a (ESI†) for $NdNiO_3$ across its T_{MIT}. At low f_{AC}, *e.g.*, 100 Hz, the R'–T was similar to the respective direct current properties, and therefore the T_{MIT} for $NdNiO_3$ was about ~130 K as shown in Fig. S7b (ESI†). In Fig. S7c (ESI†), the R'–R'' core–core curves for $NdNiO_3$ are further compared at various temperatures. In general, the temperature dependence of both their R'–T and R'–f_{AC} dependences were observed to be rather small for the metallic phase of $NdNiO_3$, which was similar to the situation observed for Cu as shown in Fig. S3 (ESI†). It is also worth noting that across the T_{MIT} the diameter of the core–core curves of $NdNiO_3$ experience an abrupt reduction (Fig. S7c, ESI†), and this indicated the response to its metal to insulator transitions from the perspective of AC-transportations.

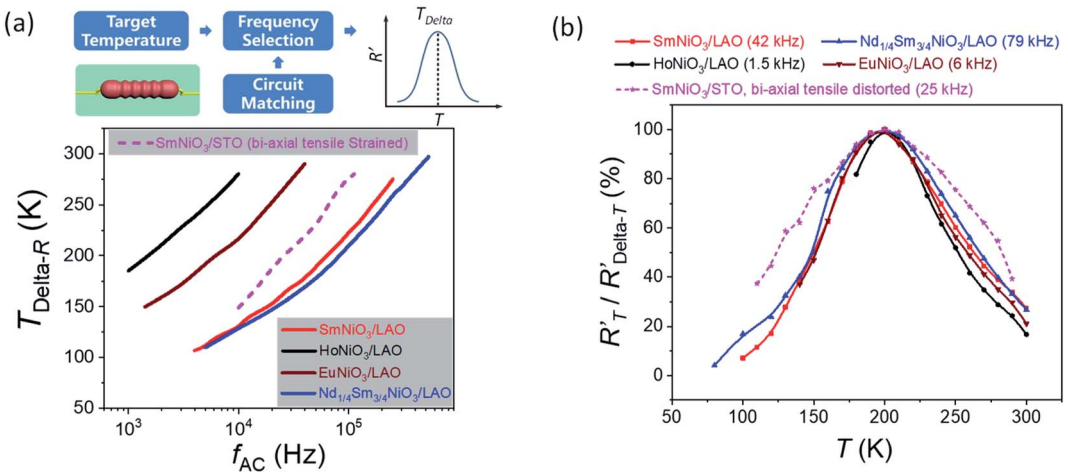

Fig. 4 (a) The required AC-frequency to achieve the desired T_{Delta} when using $ReNiO_3$ thin films at various rare-earth compositions and states of interfacial strains as a T_{Delta}-thermistor is summarized. The upper figure illustrates the principle of applying the T_{Delta}-thermistor in an electronic circuit. (b) A representative case for locking 200 K (the lowest temperature in the Arctic) utilizing the T_{Delta}-thermistor of various $ReNiO_3$ thin films.

Establishing the general rule of T_{Delta}–f_{AC}, from the materials' aspects

In Fig. 4a, the respective T_{Delta}–f_{AC} relationships when using $SmNiO_3/LaAlO_3$, $EuNiO_3/LaAlO_3$, $HoNiO_3/LaAlO_3$, $Sm_{3/4}Nd_{1/4}NiO_3/LaAlO_3$ and $SmNiO_3/SrTiO_3$ (tensile strained) as T_{Delta}-thermistors are summarized. From the electronic perspective to achieve active regulation, it was possible for the T_{Delta} to be elevated by increasing the f_{AC} for each individual $ReNiO_3$. In addition, from the perspective of materials' design, it was also possible to lower the required frequency for locking in the same T_{Delta} of $ReNiO_3$ by utilizing a smaller rare-earth element or establishing biaxial tensile distortions. This increases the flexibility to provide practical electronic applications, *e.g.*, to lock in the same maximum point in the delta-shaped R–T tendency (or T_{Delta}) *via* different combinations of the $ReNiO_3$ materials and electronically applied f_{AC}. Fig. 4b demonstrates a representative example for achieving $T_{Delta} = 200$ K, *e.g.*, the lowest temperature which is found in the Arctic, for using various $ReNiO_3$ materials. The $ReNiO_3/LaAlO_3$ with a smaller Re requires a lower f_{AC} to achieve the same T_{Delta}, and the as-achieved delta-shape in the R'–T tendency was observed to be narrower. In contrast, although the tensile strained $SmNiO_3/SrTiO_3$ required a lower f compared to $SmNiO_3/LaAlO_3$ to achieve the same T_{Delta}, the achievable delta-shape in the R'–T tendency was broader. Utilizing the peak R′ in the T_{Delta}-thermistor it was possible to lock in the respective temperature region near T_{Delta} for stabilizing the electronic working circuit or devices.

4. Conclusions

In conclusion, assisted by temperature dependent NEXAFS it was demonstrated that elevating the temperature strengthens the insulating phase of $ReNiO_3$ that enhances not only the electrical conductivity but also their Coulomb viscosity. The Coulomb viscosity moderates the temperature dependence in the real part resistivity and relaxation frequency that further results in crosslinking of the R'–f_{AC} curves measured at adjacent temperatures and enables electronic switchability between NTCR-, T_{Delta}- and PTCR-thermistor transports by simply regulating f_{AC} without varying the material constitutions or device structure. It is worth noting that the T_{Delta}-thermistor exhibits a maxima in the R'–T tendency that is useful for locking in specific temperatures. From the electronic perspective the T_{Delta} can be further actively elevated by increasing the f_{AC} for a given composition of $ReNiO_3$ over a broad range of temperatures. Furthermore, from the perspective of materials' design, the T_{Delta}–f_{AC} relationship as well as the switching frequencies between NTCR-, T_{Delta}- and PTCR-thermistors can be widely adjusted *via* the rare-earth composition and status of the interfacial strains. Combining both aspects of AC electronic and materials' designs provides large flexibility to cater for intelligent temperature sensing in practical applications.

Availability of data

The data that support the findings of this study are available from the corresponding authors upon request.

Author contributions

Jikun Chen proposed the original scientific idea, planned the work, partially performed the experiment (*i.e.*, sample growth, structure and transport characterizations), analysed the data, and wrote the manuscript. Haifan Li contributed in the transport characterizations under the supervision of Jikun Chen. Jiaou Wang contributed for the TDEXAFS experiment. Xinyou Ke assisted in the writing of the manuscript and provided constructive suggestions. Jinhao Chen contributed to the sample growth under the supervision of Jikun Chen. Hongliang Dong and Binghui Ge contributed to the TEM experiment. Nuofu Chen and Yong Jiang provided support for the aspects of sample growth and characterization, respectively.

Conflicts of interest

We declare no competing financial interest.

Acknowledgements

This work was supported by National Natural Science Foundation of China (No. 61674013) and the Beijing New-star Plan of Science and Technology (No. Z191100001119071).

References

1 Z. Zhang, D. Schwanz, B. Narayanan, M. Kotiuga, J. A. Dura, M. Cherukara, H. Zhou, J. W. Freeland, J. Li, R. Sutarto, F. He, C. Wu, J. Zhu, Y. Sun, K. Ramadoss, S. S. Nonnenmann, N. Yu, R. Comin, K. M. Rabe, S. K. R. S. Sankaranarayanan and S. Ramanathan, Rerovskite nickelates as electric-field sensor in salt water, *Nature*, 2018, **553**, 68.

2 H. T. Zhang, F. Zuo, F. Li, H. Chan, Q. Wu, Z. Zhang, B. Narayanan, K. Ramadoss, I. Chakraborty, G. Saha, G. Kamath, K. Roy, H. Zhou, A. A. Chubykin, S. K. R. S. Sankaranarayanan, J. H. Choi and S. Ramanathan, Perovskite nickelates as bio-electronic interfaces, *Nat. Commun.*, 2019, **10**, 1651.

3 Y. Zhou, X. Guan, H. Zhou, K. Ramadoss, S. Adam, H. Liu, S. Lee, J. Shi, M. Tsuchiya, D. D. Fong and S. Ramanathan, Strongly correlated perovskite fuel cells, *Nature*, 2016, **534**, 231.

4 J. Shi, Y. Zhou and S. Ramanathan, Colossal resistance switching and band gap modulation in a perovskite nickelate by electron doping, *Nat. Commun.*, 2014, **5**, 4860.

5 F. Zuo, P. Panda, M. Kotiuga, J. Li, M. Kang, C. Mazzoli, H. Zhou, A. Barbour, S. Wilkins, B. Narayanan, M. Cherukara, Z. Zhang, S. K. R. S. Sankaranarayanan, R. Comin, K. M. Rabe, K. Roy and S. Ramanathan, Habituation based synaptic plasticity and organismic learning in a quantum perovskite, *Nat. Commun.*, 2017, **8**, 240.

6 G. Catalan, Progress in perovskite nickelate research, *Phase Transitions*, 2008, **81**, 729.

7 J. Shi, S. D. Ha, Y. Zhou, F. Schoofs and S. Ramanathan, A correlated nickelate synaptic transistor, *Nat. Commun.*, 2013, **4**, 2676.
8 T. Yajima, T. Nishimura and A. Toriumi, Positive-bias gate-controlled metal–insulator transition in ultrathin VO_2 channels with TiO_2 gate dielectrics, *Nat. Commun.*, 2015, **6**, 10104.
9 J. A. Alonso, J. L. García-Muñoz, M. T. Fernández-Díaz, M. A. G. Aranda, M. J. Martínez-Lope and M. T. Casais, Charge Disproportionation in $RNiO_3$ Perovskites: simultaneous metal-insulator and structural transition in $YNiO_3$, *Phys. Rev. Lett.*, 1999, **82**, 3871.
10 I. I. Mazin, D. I. Khomskii, R. Lengsdorf, J. A. Alonso, W. G. Marshall, R. M. Ibberson, A. Podlesnyak, M. J. Martínez-Lope and M. M. Abd-Elmeguid, Charge Ordering as Alternative to Jahn-Teller Distortion, *Phys. Rev. Lett.*, 2007, **98**, 176406.
11 K. Martens, J. W. Jeong, N. Aetukuri, C. Rettner, N. Shukla, E. Freeman, D. N. Esfahani, F. M. Peeters, T. Topuria, P. M. Rice, A. Volodin, B. Douhard, W. Vandervorst, M. G. Samant, S. Datta and S. S. P. Parkin, Field effect and strongly localized carriers in the metal-insulator transition material VO_2, *Phys. Rev. Lett.*, 2015, **115**, 196401.
12 J. D. Budai, J. Hong, M. E. Manley, E. D. Specht, C. W. Li, J. Z. Tischler, D. L. Abernathy, A. H. Said, B. M. Leu, L. A. Boatner, R. J. McQueeney and O. Delaire, Metallization of vanadium dioxide driven by large phonon entropy, *Nature*, 2014, **515**, 535.
13 J. Chen, H. Hu, J. Wang, T. Yajima, B. Ge, X. Ke, H. Dong, Y. Jiang and N. Chen, Overcoming synthetic metastabilities and revealing metal-to-insulator transition & thermistor bi-functionalities for d-band correlation perovskite nickelates, *Mater. Horiz.*, 2019, **6**, 788.
14 J. Chen, H. Hu, J. Wang, C. Liu, X. Liu, Z. Li and N. Chen, A d-band electron correlated thermoelectric thermistor established in metastable Perovskite family of rare-earth nickelates, *ACS Appl. Mater. Interfaces*, 2019, **11**, 34128–34134.
15 R. Jaramillo, S. D. Ha, D. M. Silevitch and S. Ramanathan, Origins of bad-metal conductivity and the insulator–metal transition in the rare-earth nickelates, *Nat. Phys.*, 2014, **10**, 304.
16 K. Ramadoss, N. Mandal, X. Dai, Z. Wan, Y. Zhou, L. Rokhinson, Y. P. Chen, J. Hu and S. Ramanathan, Sign reversal of magnetoresistance in a perovskite nickelate by electron doping, *Phys. Rev. B*, 2016, **94**, 235124.
17 Y. Huang, K. Wu, Z. Xing, C. Zhang, X. Hu, P. Guo, J. Zhang and J. Li, Understanding the validity of impedance and modulus spectroscopy on exploring electrical heterogeneity in dielectric ceramics, *J. Appl. Phys.*, 2019, **125**, 084103.
18 M. Younas, M. Nadeem, M. Atif and R. Grossinger, Metal-semiconductor transition in $NiFe_2O_4$ nanoparticles due to reverse cationic distribution by impedance spectroscopy, *J. Appl. Phys.*, 2011, **109**, 093704.
19 R. Tang, C. Jiang, J. Jian, Y. Liang, X. Zhang, H. Wang and H. Yang, Impedance spectroscopy and scaling behaviors of $Sr_3Co_2Fe_{24}O_{41}$ hexaferrite, *Appl. Phys. Lett.*, 2015, **106**, 022902.
20 X. Xie, Z. Zhou, T. Wang, R. Liang and X. Dong, High temperature impedance properties and conduction mechanism of W^{6+}-doped $CaBi_4Ti_4O_{15}$ Aurivillius piezoceramics, *J. Appl. Phys.*, 2018, **124**, 204101.
21 A. Khodorov, S. A. S. Rodrigues, M. Pereira and M. J. M. Gomes, Impedance spectroscopy study of a compositionally graded lead zirconate titanate structure, *J. Appl. Phys.*, 2007, **102**, 114109.
22 H. Rahmouni, M. Nouiri, R. Jemai, N. Kallel, F. Rzigua, A. Selmi, K. Khirouni and S. Alaya, Electrical conductivity and complex impedance analysis of 20% Ti-doped $La_{0.7}Sr_{0.3}MnO_3$ perovskite, *J. Magn. Magn. Mater.*, 2007, **316**, 23–28.
23 H. Rahmouni, M. Smari, B. Cherif, E. Dhahrib and K. Khirouni, Conduction mechanism, impedance spectroscopic investigation and dielectric behavior of $La_{0.5}Ca_{0.5-x}Ag_xMnO_3$ manganites with compositions below the concentration limit of silver solubility in perovskites ($0 \leq x \leq 0.2$), *Dalton Trans.*, 2015, **44**, 10457–10466.
24 S. J. Lee, K. Y. Kang and S. K. Han, Low-frequency dielectric relaxation of BaTiO3 thin-film capacitors, *Appl. Phys. Lett.*, 1999, **75**, 1784–1786.
25 K. Kleiner, J. Melke, M. Merz, P. Jakes, P. Nage, S. Schuppler, V. Liebau and H. Ehrenberg, Unraveling the degradation process of $LiNi_{0.8}Co_{0.15}Al_{0.05}O_2$ electrodes in commercial lithium ion batteries by electronic structure investigations, *ACS Appl. Mater. Interfaces*, 2015, **7**, 19589.
26 L. A. Montoro, M. Abbate and J. M. Rosolen, Electronic structure of transition metal Ions in deintercalated and reintercalated $LiCo_{0.5}Ni_{0.5}O_2$, *J. Electrochem. Soc.*, 2000, **147**, 1651–1657.
27 J. Chen, W. Mao, B. Ge, J. Wang, X. Ke, V. Wang, Y. Wang, M. Döbeli, W. Geng, H. Matsuzaki, J. Shi and Y. Jiang, Revealing the role of lattice distortions in the hydrogen-induced metal-insulator transition of $SmNiO_3$, *Nat. Commun.*, 2019, **10**, 694.
28 E. Ohg, Negative temperature coefficient resistance (NTCR) ceramic thermistors: an industrial perspective, *J. Am. Ceram. Soc.*, 2009, **92**, 967–983.
29 A. Rogalski, Infrared detectors: an overview, *Infrared Phys. Technol.*, 2002, **43**, 187–210.
30 F. Y. Bruno, K. Z. Rushchanskii, S. Valencia, Y. Dumont, C. Carrétéro, E. Jacquet, R. Abrudan, S. Blügel, M. Ležaić, M. Bibes and A. Barthélémy, Rationalizing strain engineering effects in rare-earth nickelates, *Phys. Rev. B: Condens. Matter Mater. Phys.*, 2013, **88**, 195108.
31 F. Conchon, A. Boulle and R. Guinebretière, Effect of tensile and compressive strains on the transport properties of $SmNiO_3$ layers epitaxially grown on (001) $SrTiO_3$ and $LaAlO_3$ substrates, *Appl. Phys. Lett.*, 2007, **91**, 192110.
32 S. D. Ha, R. Jaramillo, D. M. Silevitch, F. Schoofs, K. Kerman, J. D. Baniecki and S. Ramanathan, Hall effect measurements on epitaxial SmNiO3 thin films and implications for antiferromagnetism, *Phys. Rev. B: Condens. Matter Mater. Phys.*, 2013, **87**, 125150.